catalysts

MDPI

Article

Effect of pH on Microstructure and Catalytic Oxidation of Formaldehyde in MnO_2 Catalyst

Wenrui Zhang [1,*], Meilu Hao [1], Yonghui Wang [1], Pengfei Sun [1], Dongjuan Zeng [1], Xinya Wang [1] and Peng Liang [2,*]

[1] College of Safety and Environmental Engineering, Shandong University of Science and Technology, Qingdao 266590, China
[2] College of Chemical and Biological Engineering, Shandong University of Science and Technology, Qingdao 266590, China
* Correspondence: wenrui.mao@163.com (W.Z.); liangpeng202@hotmail.com (P.L.); Tel.: +86-15253263237 (W.Z.); +86-13678890728 (P.L.)

Abstract: Layered δ-MnO_2 catalysts were prepared using the one-step redox method in precursor solutions with five different pH values (pH = 7, 9, 11, 13, and 14). The effects of pH on the physical properties and catalytic activity of the catalyst were investigated through XRD, SEM, TEM, BET, XPS, H_2-TPR, and HCHO degradation tests at room temperature. The results showed that the layer spacing, manganese vacancy content, Mn^{4+}/Mn^{3+} ratio, and surface-reactive oxygen species content of MnO_2 increased with the increase in pH value in the alkaline range. When the catalyst was prepared at pH = 13, the above characteristics of the catalyst reached the optimal value which contributed to the high catalytic activity. Combined with the related characterization results, it was proved that changing the pH can affect the degree of oxidation in the catalyst synthesis process, increase the number of active oxygen and the oxygen mobility of the catalyst, and effectively improve the catalytic activity of the manganese dioxide catalyst for HCHO. This work represents a giant step toward the preparation of an effective catalyst for practical applications of HCHO removal at room temperature at a low concentration and high velocity.

Keywords: δ-MnO_2; pH; formaldehyde; manganese vacancy; surface-reactive oxygen species

Citation: Zhang, W.; Hao, M.; Wang, Y.; Sun, P.; Zeng, D.; Wang, X.; Liang, P. Effect of pH on Microstructure and Catalytic Oxidation of Formaldehyde in MnO_2 Catalyst. *Catalysts* **2023**, *13*, 490. https://doi.org/10.3390/catal13030490

Academic Editors: Florica Papa, Anca Vasile and Gianina Dobrescu

Received: 8 January 2023
Revised: 14 February 2023
Accepted: 21 February 2023
Published: 28 February 2023

1. Introduction

Formaldehyde (HCHO) is a major indoor air pollutant released by furniture and decorative materials [1]. It is highly toxic. Short exposure can cause a series of nervous, respiratory, and skin allergy problems. Long-term exposure has carcinogenic and teratogenic effects and seriously endangers human health [2]. Catalytic oxidation technology with a metal oxide catalyst as the core can transform HCHO into harmless small-molecule CO_2 and H_2O, which has become one of the effective means to eliminate indoor formaldehyde [3]. Manganese oxides (MnO_x) are widely used in the removal of HCHO due to their high activity, low toxicity, and easy availability [4]. The preparation method has a great influence on the catalytic performance. Excellent performance in a catalyst (photocatalyst, electrocatalyst, thermocatalysis, etc.) can be attained by adjusting different preparation parameters [5–9]. The redox method is commonly used to prepare manganese oxides, which generates specific MnO_x via the redox reaction between the manganese source precursor ($KMnO_4$) and the specific reducing agent ($MnSO_4$ and $Mn(NO_3)_2$) [10–12].

This study shows that adjusting the preparation parameters of the redox method has an important impact on the crystal morphology, microstructure, redox property, and the degradation activity of the target pollutants of the MnO_x catalyst. The redox reaction time can change the MnO_x catalyst morphology and then affect the removal efficiency of formaldehyde. Pang et al. [13] mixed $KMnO_4$ with HNO_3 and $Ce(NO_3)_3{\cdot}H_2O$ in an autoclave and heated the reaction at 140 °C to prepare manganese dioxide (MnO_2). Solid, nanoflake, and hollow MnO_2 microspheres were obtained by adjusting the reaction time

(1 h, 3 h, and 4 h). The hollow manganese dioxide showed the best effect on formaldehyde due to its large pore size and high oxidation state. Secondly, the mixture ratio of reaction materials in the preparation process also dramatically influenced the catalyst's physical and chemical properties. Wu et al. [14] prepared α-MnO_2 by adding $Mn(NO_3)_2$ and KOH to a $KMnO_4$ solution and found that the catalyst prepared at a calcination temperature of pH = 8 and 400 °C could 100% convert o-xylene to CO_2 at 220 °C, which was 50 °C lower than the previous traditional precipitation method. A high content of Mn^{4+} is beneficial to the catalytic oxidation of o-xylene. Min et al. prepared δ-MnO_2 for the degradation of gaseous toluene by adjusting different molar ratios of $KMnO_4$ and $MnSO_4 \cdot H_2O$ [15]. The experimental results showed that when the molar ratio was 2.9–3.7, α@δ-MnO_2 had the primary catalytic activity for toluene. At this time, the specific surface area and oxygen vacancy of the catalyst were greatly increased owing the α-δ phase ratio being close. So, the catalyst had excellent oxygen absorption and storage capacity. In addition, heating in solution is one of the redox synthesis processes of catalysts. The temperature and the precursor solution pH significantly affect the properties and activity of the catalyst. Chen et al. [16] reacted $KMnO_4$ with H_2SO_4, HCl, HNO_3, and $C_2H_4O_2$ at different temperatures (60–90 °C), and the molar ratio of potassium permanganate to acid was 1:5. The experimental results showed that MnO_4^- with an oxidizing property and Cl^- with a reducing property reacted with MnO_4^- to form Mn^{2+} in 4 mol/L HCl at 60 °C. At low temperature, Mn^{2+} reacted with MnO_4^- to form [MnO_x] structural moieties and then layered δ-MnO_2 microspheres through condensation polymerization. Nevertheless, in 10 mol/L $C_2H_4O_2$ at 95 °C, due to the higher temperature and stronger acid concentration, the bonding between K^+ and water molecules was reduced which enlarged the interlayer spacing of δ-MnO_2 and destroyed the interlayer [K-H_2O]$^+$ hydrated ions. Finally, the layered structure of δ-MnO_2 collapsed and formed the α-MnO_2 tunnel structure which reduced the reactivity. Jiang et al. [17] used K_2FeO_4 and $MnSO_4$ to prepare MnO_2 through simple redox reactions and subjected it to different acidifications (H_2SO_4, HNO_3, and HAc). The results showed that the acid treatment effectively increased the number of acidic sites of MnO_2, which can enhance the adsorption of NH_3 and the activity of the NH_3-SCR reaction. It is easy to find that the acid–base property of the precursor is one of the key factors for preparing high-performance catalysts.

Researchers have investigated the effect of acidic conditions or acid treatment on the relationship between the structure and performance of MnO_x catalysts at present. However, the effects of alkaline conditions on the structural defects, active sites and redox properties of MnO_x have not been systematically studied. Based on the previous research of a MnO_2 catalyst prepared with the one-step oxidation and reduction method, we further studied the effect of pH on the microstructure and surface properties of MnO_x by modulating the pH of the precursor solution (7, 9, 11, 13, 14) with XRD, SEM, TEM, BET, XPS and H_2-TPR. Furthermore, the optimal pH conditions for the preparation of MnO_x catalysts with excellent catalytic performance of HCHO oxidation at room temperature were explored and the effect mechanism was explained.

2. Results and Discussion

2.1. Influence of pH Value on Catalyst Performance

Under the conditions of 25 °C, GHSV = 16 × 10^4 h^{-1}, RH = 40%, and the initial concentration of HCHO = 4.02 mg/m^3; the catalytic oxidation activities of five catalysts prepared under different alkaline conditions were investigated and are shown in Figure 1. Additionally, the catalytic removal efficiency of each catalyst for formaldehyde at 5.5 h and 10 h is shown in Table 1. From Figure 1 and Table 1, it can be seen that different alkaline conditions impacted the catalytic activity of HCHO, and the activity decreased in the order of 13-MnO_2 > 11-MnO_2 > 9-MnO_2 > 7-MnO_2 > 14-MnO_2. Among them, the catalyst prepared at pH 13 had the best catalytic effect. With the enhancement of solution alkalinity, the catalytic activity and stability of MnO_2 on HCHO were enhanced. However, when the pH of the solution increased to 14, the catalytic activity was significantly weakened. This

indicated that a high concentration of hydroxide would inhibit the activity of the catalyst. The efficiency of 7-MnO_2 synthesized under neutral conditions (pH = 7) began to decrease at the second hour. The conversion rate of 13-MnO_2 to HCHO could be maintained at 100% for the first 6 h and declined after 6 h. The above results indicated that introducing an appropriate amount of hydroxide could effectively improve the catalytic activity of MnO_2.

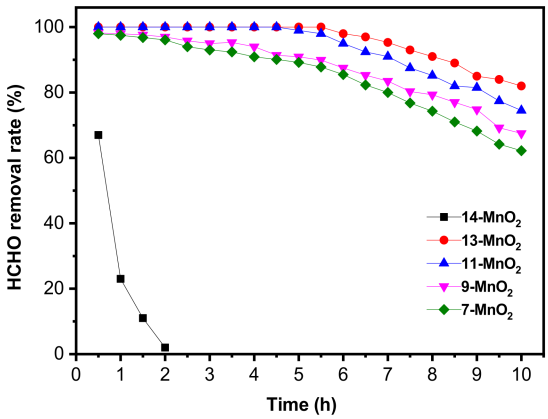

Figure 1. Influence of pH on catalytic activity; reaction conditions: reaction temperature = 25 °C, GHSV = 16 × 10^4 h^{-1}, RH = 40%, initial concentration of HCHO = 4.02 mg/m^3.

Table 1. List of $R_{5.5\,h}$ and $R_{10\,h}$ for each catalyst.

Samples	$R_{5.5\,h}$/%	$R_{10\,h}$/%
7-MnO_2	87.8	62.2
9-MnO_2	89.9	67.5
11-MnO_2	98	74.2
13-MnO_2	100	82.9
14-MnO_2	0	0

Note: $R_{5.5\,h}$ refers to the conversion rate of formaldehyde when the continuous reaction time was 5.5 h. $R_{10\,h}$ refers to the conversion rate of formaldehyde when the continuous reaction time was 10 h.

2.2. Influence of Space Velocity on Catalytic Effect

In industrial applications, airspeed is an essential factor affecting the miniaturization of air purification systems and efficiency. From the results in Section 2.1, it was found that the catalytic activity of the 13-MnO_2 catalyst was significantly improved. At room temperature (25 °C) and an initial concentration of HCHO of 4.02 mg/m^3, the effects of different space speeds (8 × 10^4 h^{-1}, 12 × 10^4 h^{-1}, and 16 × 10^4 h^{-1}) within 10 h on the catalytic degradation of HCHO by the 13-MnO_2 catalyst was investigated (shown in Figure 2). When the space speed was 8 × 10^4 h^{-1} and 12 × 10^4 h^{-1}, the removal rate of HCHO by the 13-MnO_2 catalyst reached 100%; when the space velocity rose to 16 × 10^4 h^{-1}, the catalyst efficiency slightly decreased after 6 h but this remained greater than 85%. Part of the HCHO was taken out of the reactor before fully contacting with the catalyst with the increase in space velocity, resulting in the effective contact time between the reactant and the active center of the catalyst being reduced. Additionally, the reduction of reactant amount led to an insufficient catalytic reaction, which caused a slight reduction in the catalytic activity. Generally, the 13-MnO_2 catalyst can maintain excellent catalytic activity at room temperature, low concentration, and high velocity, which has played a certain role in promoting the design and development of indoor small air purifiers.

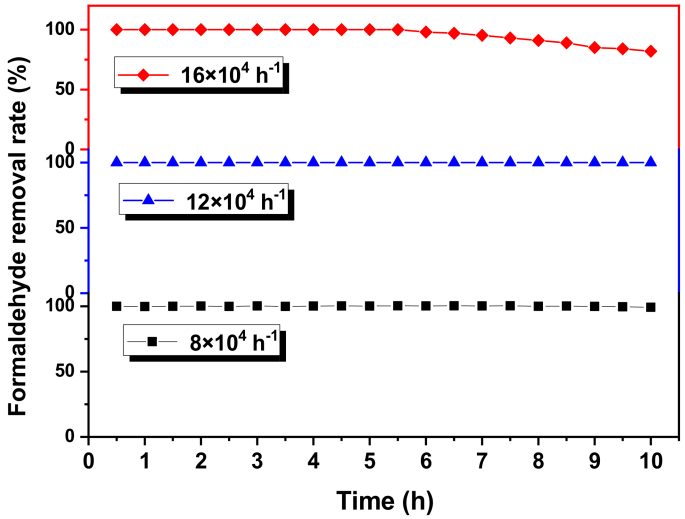

Figure 2. Degradation efficiency of 13-MnO_2 on HCHO at different space speeds; reaction conditions: reaction temperature = 25 °C, initial concentration of HCHO = 4.02 mg/m^3, RH = 40%.

3. Analysis and Characterization of Catalysts under Different Preparation Conditions

3.1. X-ray Diffraction (XRD)

XRD can be used to analyze the material phase structure information. The crystallography and crystallinity of MnO_2 were determined using monochromatic X-ray irradiation followed by strong X-ray diffraction in some special directions. The stronger the diffraction peak, the better the crystallinity of the material. The diffraction peaks at different angles correspond to different crystal faces of the material. XRD analysis was performed on the crystal structures of catalysts prepared under different pH conditions, and the results are shown in Figure 3. The diffraction peaks of the prepared samples were concentrated at 12.1°, 24.6°, 36.5°, and 65.5°, which belonged to the (001), (002), (100), and (110) surfaces of the sodium manganese ore type (JCPDS No.80-1098), respectively. Among the four diffraction peaks, the peak shape at 12.1° indicated that the (001) plane held a leading post, indicating that the synthesized catalysts were all layered birnessite manganese MnO_2 (δ-MnO_2) [18,19]. Among them, 7-MnO_2, 9-MnO_2, 11-MnO_2, and 13-MnO_2 catalysts had wide diffraction peaks and weak intensity, while 14-MnO_2 had narrow diffraction peaks and strong intensity. Combined with the activity results, the strong crystallinity of 14-MnO_2 was not conducive to the reaction of HCHO. In addition, the 2θ diffraction angles of 7-MnO_2, 9-MnO_2, 11-MnO_2, 13-MnO_2, and 14-MnO_2 on the (001) crystal plane were 12.08°, 12.06°, 12.01°, 11.93°, and 12.37°, respectively. According to the Bragg equation, $2d\sin\theta = n\lambda$ [20], the size of the layer spacing order of the five catalysts was 13-MnO_2 (0.687 nm) > 11-MnO_2 (0.675 nm) > 9-MnO_2 (0.663 nm) > 7-MnO_2 (0.655 nm) > 14-MnO_2 (0.651 nm). Combined with the results of catalytic activity in Section 2.1, it can be speculated that the larger the catalyst layers' spacing, the more conducive to the diffusion and adsorption of HCHO molecules in the reaction process, and the better the catalyst activity.

3.2. Scanning Electron Microscope (SEM)

An SEM was used to observe the morphology of δ-MnO_2 samples prepared under different alkaline conditions. The morphological characteristics of the prepared materials can be revealed and the role of the catalyst in the catalytic process can be inferred from the morphological appearance. As exhibited in Figure 4, 7-MnO_2, 9-MnO_2, 11-MnO_2 and 13-MnO_2 samples were nanospheres formed by the self-assembly of each nanosheet. The nanosheet had a smooth surface, flat edge, and regular shape. When the pH of the solution reached 14, the nanosheet disappeared and the surface of the nanoparticles became dense. Studies showed that the nanosheet structure increased the specific surface area of the catalyst, which was beneficial to improving the exposed active sites of the heterogeneous

catalytic reaction [21]. Therefore, the morphology of 7-MnO_2, 9-MnO_2, 11-MnO_2, and 13-MnO_2 samples was more conducive to the gas–solid catalytic reaction.

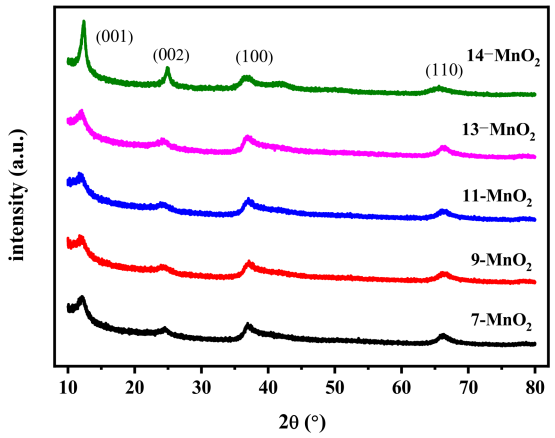

Figure 3. XRD patterns of the catalysts.

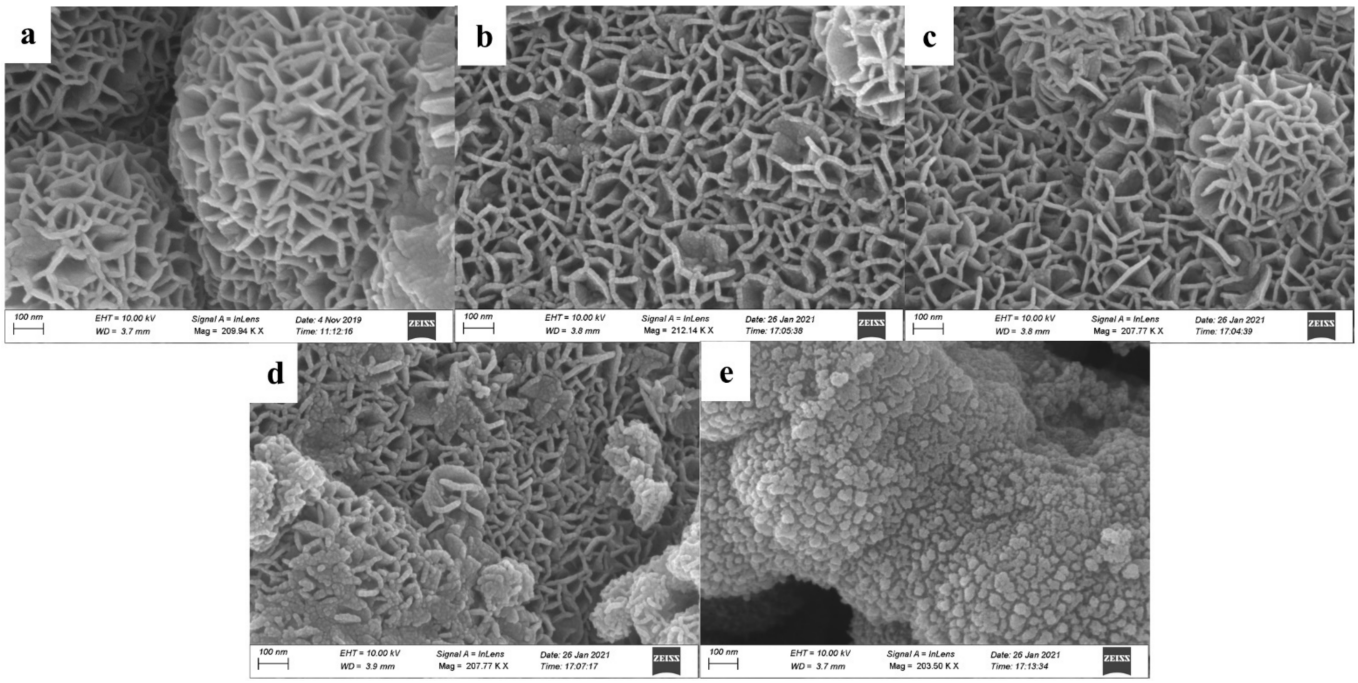

Figure 4. SEM images of the catalysts: (**a**) 7-MnO_2, (**b**) 9-MnO_2, (**c**) 11-MnO_2, (**d**) 13-MnO_2, and (**e**) 14-MnO_2.

3.3. Transmission Electron Microscopy (TEM)

TEM can be used to observe the submicroscopic structure of materials. The microstructure of the material can be observed and the influence of the structure of the catalyst on the catalytic activity can be revealed. As shown in Figure 5, δ-MnO_2 prepared at five different pH values in this study had a cluster structure composed of nanosheets as a whole. The characterization results show that the catalyst was MnO_2 with a uniform layered nanosheet structure, which was consistent with the unique two-dimensional layered tunnel structure of δ-MnO_2 reported in the literature [22,23]. The catalyst has obvious flaky structure when the pH was in the range of 7–13. When pH = 14 however, the layered structure of this cluster was destroyed. The lattice spacing of 7-MnO_2, 9-MnO_2, 11-MnO_2, 13-MnO_2, and 14-MnO_2 was 0.655 nm, 0.663 nm, 0.675 nm, 0.687 nm, and 0.651 nm, respectively. The size of the lattice spacing was arranged as 13-MnO_2 > 11-MnO_2 > 9-MnO_2 > 7-MnO_2 > 14-MnO_2. This was consistent with the XRD (001) analysis of the size of the crystal plane spacing.

Combined with the experimental activity results, it was speculated that the larger the layer spacing of manganese dioxide, the more conducive to the diffusion and adsorption of HCHO molecules in the reaction process, and the faster the catalytic reaction proceeds.

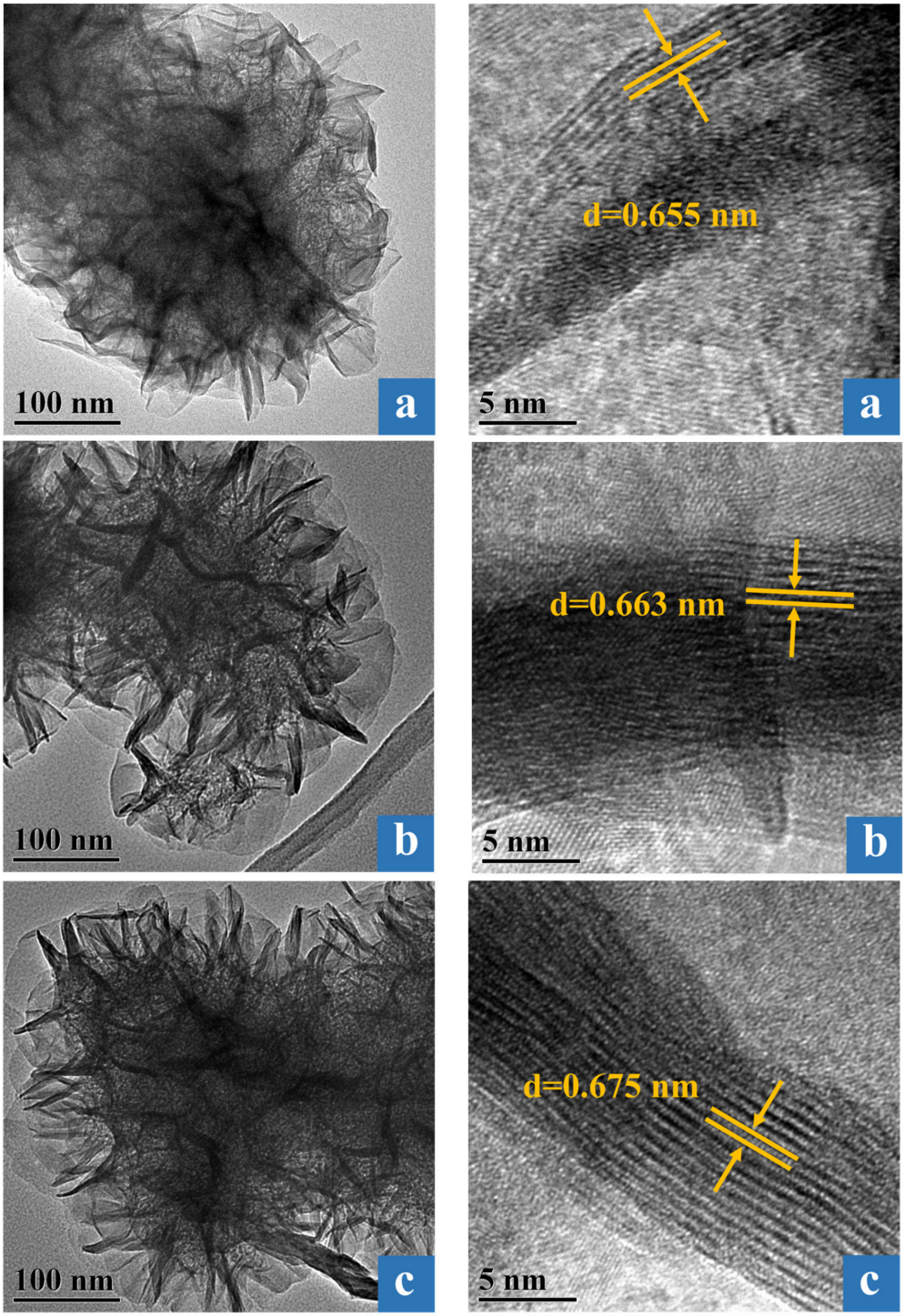

Figure 5. *Cont.*

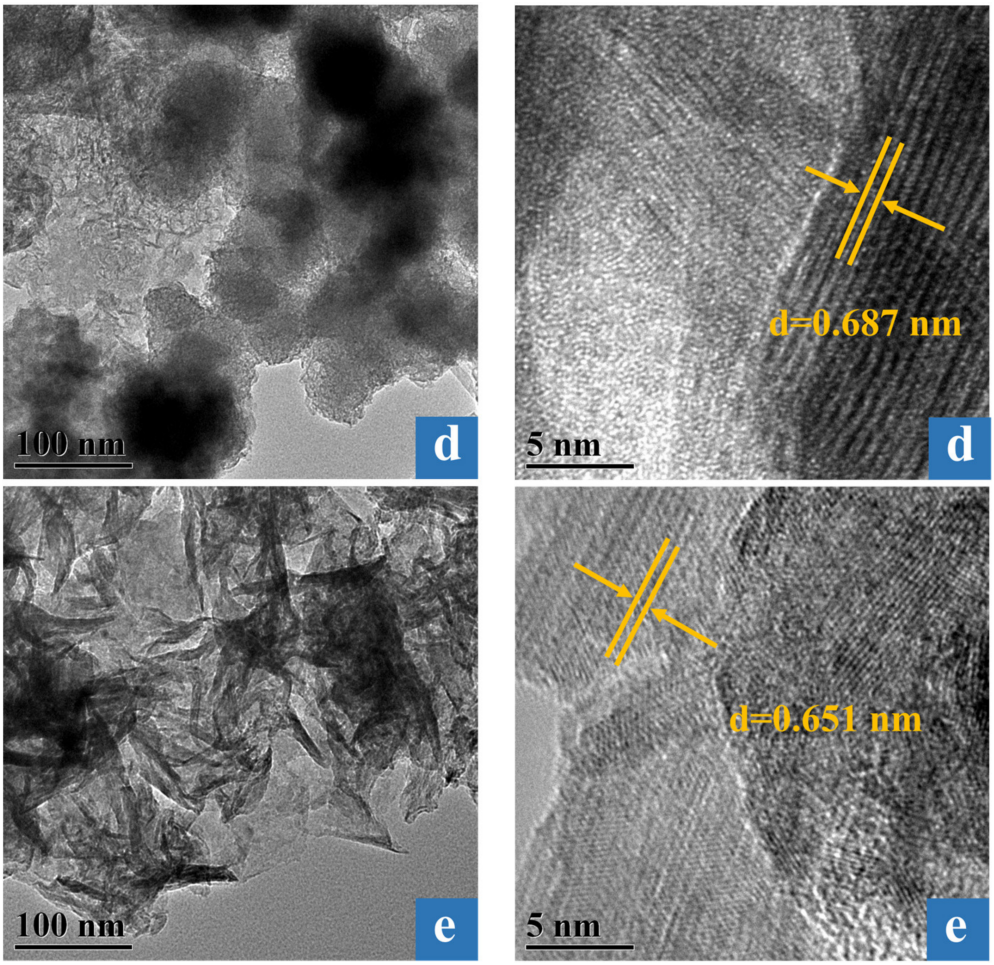

Figure 5. TEM images of the five catalysts: (**a**) 7-MnO_2, (**b**) 9-MnO_2, (**c**) 11-MnO_2, (**d**) 13-MnO_2, (**e**) 14-MnO_2.

3.4. Specific Surface Area Test (BET)

Nitrogen isotherm adsorption and desorption experiments were carried out on five MnO_2 catalysts with different pH values. In the aperture distribution diagram, the distribution of diffraction peaks indicates the size of the aperture in the material. The type of adsorption isotherm can be used to understand the distribution of pore size and particles. It can be seen from Figure 6 that the nitrogen isotherm adsorption and desorption curves of the five catalysts are all type-IV H3 hysteresis rings, which may be the slit holes formed by the accumulation of lamellar particles [24,25]. In addition, the pore sizes of the five catalysts are mainly distributed at about 3.7 nm. From Table 2, the specific surface area of the catalyst gradually decreased with increasing pH. However, when pH = 13, the specific surface area increased again and the variation law of the pore volume was the same as that of surface area. Therefore, it can be inferred that higher pH will cause the structural collapse of manganese dioxide, resulting in a reduction in the specific surface area and pore volume of the catalyst. The large specific surface area and pore volume of 13-MnO_2 increased the number of active sites whose presence facilitated the entry of HCHO and improved contact with the catalyst, which promoted the catalytic reaction efficiency of formaldehyde [19,26]. However, when the pH rose to 14, the lamellar structure of the catalyst disappeared; the specific surface area and pore size became smaller, reducing the storage space of the active species and hindering the transport and reaction of the reactant formaldehyde.

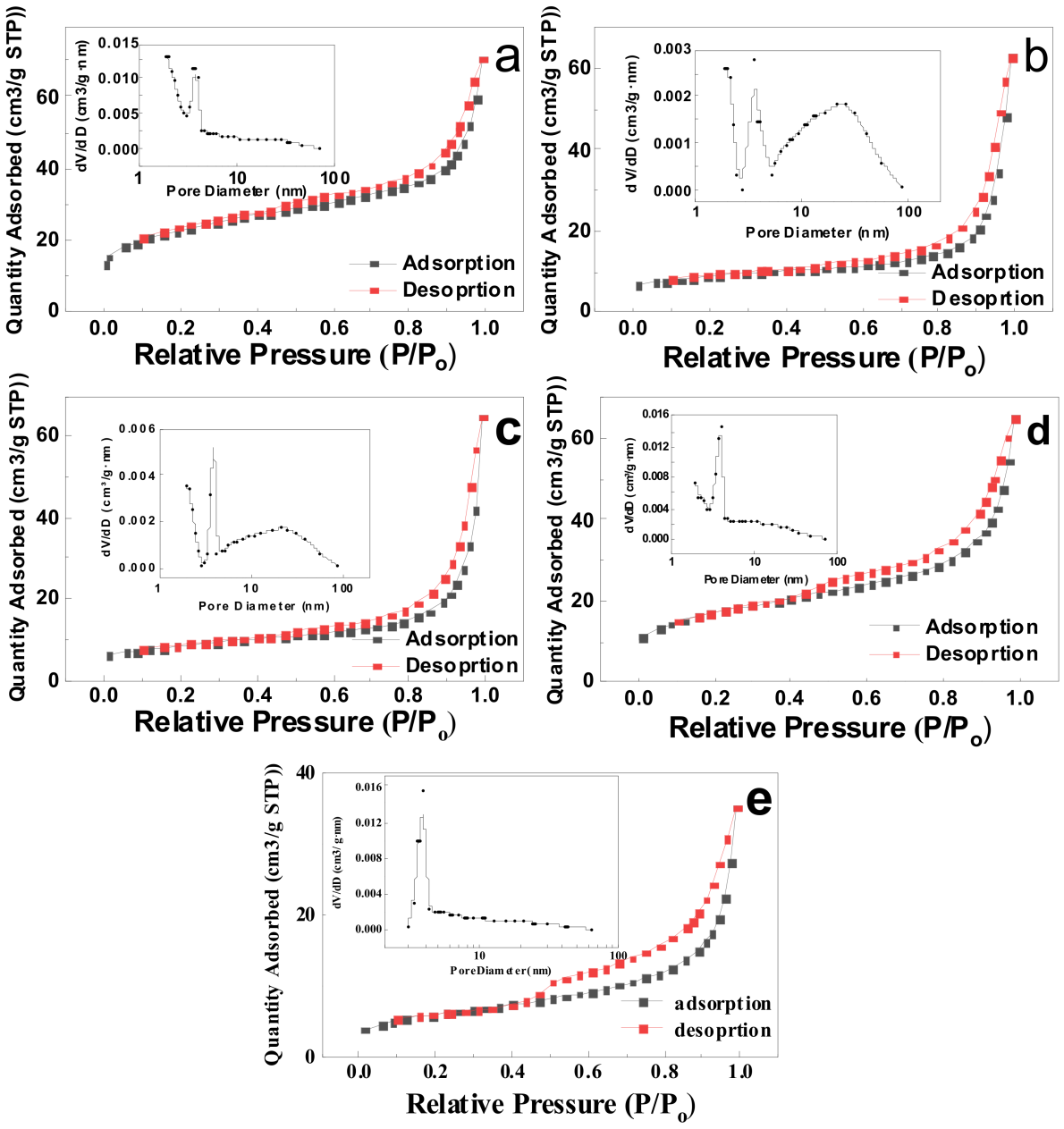

Figure 6. Nitrogen adsorption and desorption curves and pore size distribution of the five catalysts: (**a**) 7-MnO_2, (**b**) 9-MnO_2, (**c**) 11-MnO_2, (**d**) 13-MnO_2 and (**e**)14-MnO_2.

Table 2. BET specific surface area and pore volume of the five samples.

Samples	BET Surface Area (m^2/g)	Pore Volume (cm^3/g)
7-MnO_2	78.2	0.077
9-MnO_2	29.8	0.050
11-MnO_2	29.2	0.048
13-MnO_2	58.7	0.070
14-MnO_2	20.6	0.032

3.5. X-ray Photoelectron Spectroscopy (XPS)

XPS was used to test the surface chemical states of five samples under different pH conditions, as shown in Figure 7. The atomic content or relative concentration can be reflected according to the intensity of the photoelectron spectra (the area of the photoelectron peak) in the energy spectrum. The spectrum of Mn2p has two peaks at 641.8 eV and 653.5 eV,

which are Mn2p3/2 and Mn2p1/2 [27,28]. Two peaks of 642.8 eV and 641.8 eV fitted from the Mn2p3/2 peak through XPSPEAK41 software were, respectively, assigned to surface Mn^{4+} and Mn^{3+} species [29]. Mn^{4+} and Mn^{3+} on the sample surface can be quantitatively analyzed with peak area integration, and the specific values are shown in Table 3. The Mn^{4+} content on the catalyst's surface gradually increased with the growing of the pH, and the lowest and the highest Mn^{3+}/Mn^{4+} ratio were 0.69 of the 13-MnO_2 sample and 1.12 of the 14-MnO_2 sample, respectively. It can be inferred that Mn^{3+}/Mn^{4+} on the sample surface is the key to the catalytic degradation ability. Studies have shown the birnessite manganese dioxide type has a layered structure with a large number of cations between layers. According to the cation vacancy crystal structure model theory, V_{Mn} formed on the surface of MnO_2 and Mn^{3+} balances the positive charge together to make MnO_2, as a whole, appear charge-neutral [19,30]. The Mn^{3+}/Mn^{4+} ratio on the surface of the 13-MnO_2 catalyst was the lowest, indicating that the catalyst surface contained a large amount of V_{Mn} to provide active sites.

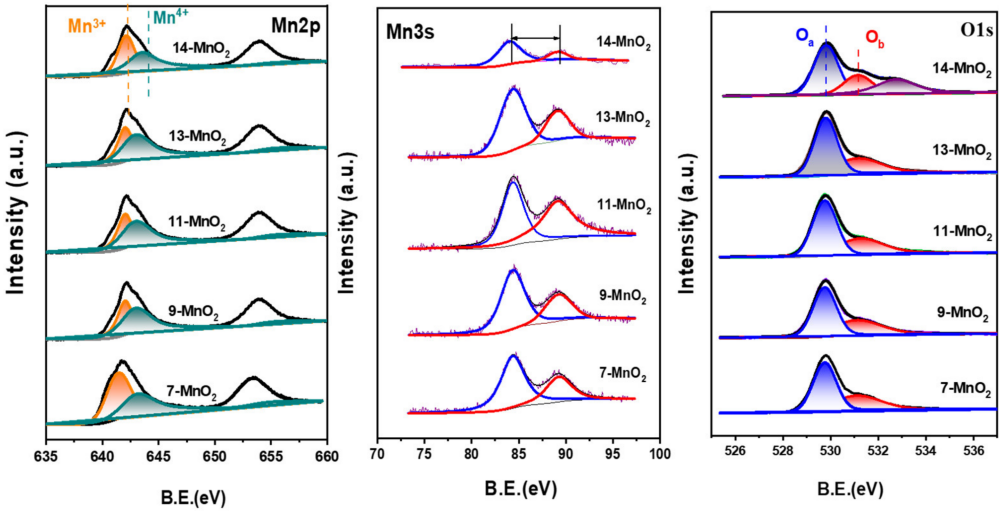

Figure 7. Mn2p, Mn3s, and O1s XPS spectra of the catalysts.

Table 3. Composition of manganese and oxygen elements on the surface of the catalyst.

Sample	Mn2p3/2	Mn3s		O1s
	Mn^{3+}/Mn^{4+}	ΔE	AOS	O_a/O_b
7-MnO_2	0.79	4.89	3.50	0.91
9-MnO_2	0.78	4.84	3.56	0.88
11-MnO_2	0.72	4.76	3.65	0.88
13-MnO_2	0.69	4.72	3.70	0.82
14-MnO_2	1.12	5.13	3.22	2.20

At the same time, we can combine the binding energy difference ΔE of the Mn3s double peaks to calculate the AOS value of the Mn atom (AOS = 9.27 − 1.18 × ΔE [31]), and the results are shown in Table 3. The AOS values of the catalysts sorted in descending order are 13-MnO_2 (3.70) > 11-MnO_2 (3.65) > 9-MnO_2 (3.56) > 7-MnO_2 (3.50) > 14-MnO_2 (3.22). The highest AOS of the 13-MnO_2 catalyst is consistent with the Mn^{3+}/Mn^{4+} rule on the sample surface in the Mn2p energy spectrum. The research shows there was a significant positive correlation between AOS value and V_{Mn} [32]. The rise in AOS value means the number of manganese vacancies increases, which provides a large number of active sites to benefit the adsorption and catalysis of HCHO. Among the five prepared catalysts with different alkalinity, the 13-MnO_2 sample exhibited better HCHO oxidation activity than other composite catalysts due to the highest V_{Mn}.

In addition, the XPS spectrum of O1s is analyzed in Figure 7. The diffraction peak at 529.6 eV can be decomposed into 529.7 eV and 531.0 eV, corresponding to lattice oxygen

(O_a) and adsorbed oxygen (O_b), respectively [33]. Studies have shown that reactive oxygen species such as -OH and O_2^- adsorbed on the catalyst surface are easier to combine with HCHO molecules and rapidly activate HCHO to chemical conversion [34,35]. From Table 3, the variation rule of O_a/O_b in these catalysts is consistent with the Mn^{3+}/Mn^{4+}: 13-MnO_2 < 11-MnO_2 < 9-MnO_2 < 7-MnO_2 < 14-MnO_2. Obviously, the content of O_b on the 13-MnO_2 catalyst surface was higher than that of O_a, indicating that 13-MnO_2 has rich species of adsorbed oxygen [30,36]. Combined with Mn2p and relevant research, oxygen coordination at large numbers of V_{Mn} on 13-MnO_2 is unsaturated, resulting in many hydroxyl and other adsorbed oxygen species at the metal vacancy [30]. These hydroxyl groups can oxidize HCHO at room temperature as the active centers of the formaldehyde oxidation reaction, resulting in the high catalytic activity of 13-MnO_2.

3.6. Temperature-Programmed Reduction of Hydrogen (H_2-TPR)

H_2-TPR can be used to analyze the redox capacity of catalysts. The reduction process of catalyst materials can be understood by fitting the diffraction peaks. The redox capacity of catalysts prepared under different pH conditions was also tested using temperature-programmed hydrogen reduction. Figure 8 shows the H_2-TPR diagram of the catalysts prepared under five different pH conditions (7, 9, 11, 13, 14). It can be seen that there are four obvious reduction peaks for each catalyst. The first reduction peak is the reduction of hydrogen by adsorbed oxygen on the surface, and the next three peaks are the reduction of $MnO_2 \rightarrow Mn_2O_3$, $Mn_2O_3 \rightarrow Mn_3O_4$, and $Mn_3O_4 \rightarrow MnO$, respectively [12,37]. The first low-temperature reduction peak temperature from small to large is in the following order: 13-MnO_2 (202 °C) < 11-MnO_2 (231 °C) < 9-MnO_2 (239 °C) < 14-MnO_2 (246 °C) < 7-MnO_2 (322 °C). It is reported that the lower the low-temperature reduction peak temperature, the stronger the reduction ability of the catalyst [38]. The reduction peak of 13-MnO_2 appears at the lowest temperature of 202 °C, which shows that 13-MnO_2 has the strongest reduction ability among the five catalysts. Furthermore, the lower surface adsorption oxygen reduction temperature can make the surface-active oxygen species more easily activated, which is beneficial to enhancing the activity of the catalyst. Moreover, the H_2-TPR results can reflect the oxygen mobility of samples. The strong reducing ability of 13-MnO_2 indicates that its catalyst has strong oxygen mobility to adsorb more surface-reactive oxygen species for redox reactions [39].

3.7. Mechanism Analysis

From the experiments, it is not difficult to find that the precursor solution's pH could affect the catalyst's physical properties and structure, which will further affect the degradation activity of formaldehyde. Therefore, combined with the characterization results and related research [20], we analyzed the mechanism of the influence of the pH of the precursor solution on the activity of layered MnO_2. As illustrated in Figure 9, with the increase in solution alkalinity, the content of Mn^{4+} in the MnO_2 catalyst increased and manganese vacancies were generated, which, together with Mn^{3+}, kept MnO_2 electrically neutral. Due to the manganese vacancy as active site, oxygen molecules in the air can be adsorbed and transformed into O_2^-, and water in the air can combine with O_2^- to form a hydroxyl group (-OH). The hydroxyl group and O_2^- can react with HCHO to degrade it to carbon dioxide and water, respectively. However, when the alkalinity of precursor solution is too high (pH = 14), the Mn-O ionic bond supporting the MnO_2 skeleton may be broken, resulting in the collapse of the layered morphology of the catalyst. Both the specific surface area and manganese vacancies numbers decreased, and the contact between the active sites and formaldehyde molecules reduced, thus leading to the decrease in activity eventually.

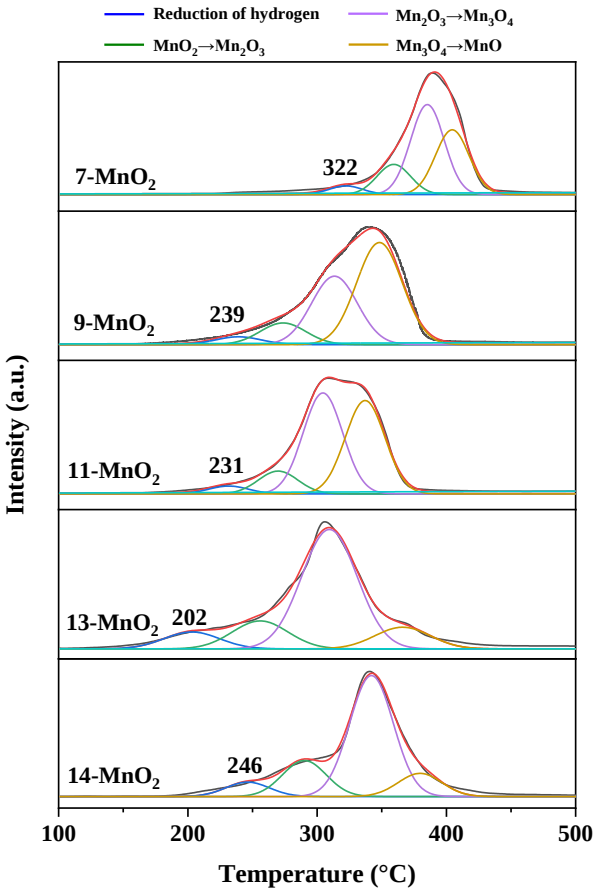

Figure 8. H_2-TPR diagram of five catalysts.

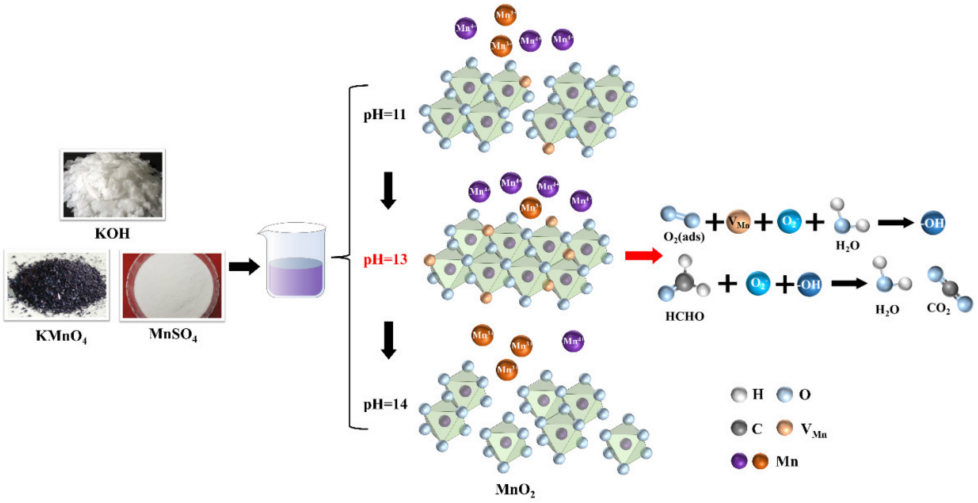

Figure 9. Schematic diagram of the mechanism of HCHO degradation by MnO_2 with different alkalinity.

4. Experiment

4.1. Preparation of Catalyst

All reagents used in the study were analytically pure. The samples were prepared via a simple redox reaction published in the previous study [40] by our group. In this part, $MnSO_4$ (purchased from Shanghai Macklin Biochemical Co., Ltd, Shanghai, China) was selected as the reducing agent, and different contents of KOH (purchased from Shanghai Macklin Biochemical Co., Ltd, Shanghai, China) were added in the synthesis process to regulate the manganese vacancy (V_{Mn}) content in the MnO_2 catalyst. Firstly, different KOH

samples were added to deionized water to obtain five parts of 200 mL of alkaline solvent with pH = 7, 9, 11, 13 and 14. Then, 2.0 g of $KMnO_4$ (purchased from Shanghai Aladdin Biochemical Technology Co., Ltd, Shanghai, China) and 1.0 g of $MnSO_4 \cdot H_2O$ were weighed (the mass ratio $KMnO_4/MnSO_4$ was 2:1). Different amounts of alkaline solvent were added to adjust the pH and stirred at room temperature until fully dissolved. The mixture was moved to a 60 °C water bath for a continuous reaction for 10 h. After natural cooling, the product was filtered, cleaned with deionized water three times, and heated and dried in 40 °C ovens for 12 h to obtain the final required products, denoted as 7-MnO_2, 9-MnO_2, 11-MnO_2, 13-MnO_2 and 14-MnO_2, respectively.

4.2. Catalyst Characterization

X-ray diffraction patterns were conducted on an X-ray diffractometer (Bruker, D8 Advance, Karlsruhe, Germany) equipped with Cu-Kα (λ = 0.5406 nm, 40 KV, 150 mA) radiation in the range of 10–80° with a step size of 5°/min. The catalyst microstructures were characterized with a scanning electron microscope (JEOL, JSM-7800F, Tokyo, Japan) with a working voltage of 10 kV and transmission electron microscopy (JEOL, JEM-2100F, Tokyo, Japan) with an acceleration voltage of 200 kV. A nitrogen isothermal adsorption and desorption curve of materials was mapped on ASAP 2020 (Micromeritics, ASAP 2020, Norcross, GA, USA) with the degassing temperature at 100 °C for 10 h to analyze the sample's specific surface area and pore volume. X-ray photoelectron spectra were collected using a Thermo ESCALAB 250Xi X-ray photoelectron spectrometer (Thermo Fisher, ESCALAB-250Xi, Waltham, MA, USA) equipped with Al Kα (284.6 eV) radiation. The temperature-programmed reduction of hydrogen was carried out on a Quantachrom automatic chemisorption analyzer (Micromeritics, ASAP 2010, Norcross, GA, USA). A sample of 0.05 g was exposed to a stream of 10% H_2/Ar mixture by volume fraction and heated from room temperature to 800 °C at a rate of 10 °C/min.

4.3. Evaluation of Catalyst Activity

As shown in Figure 10, a self-assembled microtube reactor was used in this experiment. The 100 mg catalyst was filled in a reaction tube with an inner diameter of 6 mm. The air pump directly extracted ambient air through a formaldehyde gas generator and humidification–dilution device, respectively. Additionally, then, the premixed airflow was combined in the reaction tube. The experimental gas satisfying the requirements of formaldehyde concentration, space velocity, and humidity could be obtained by adjusting the flow ratio of the two air streams. In the experiment, the inlet concentration and relative humidity (RH) were set as 4.02 mg/m^3 and 40%. The gas flow rate was 150–600 L/min, and the volume space velocity (GHSV) range was 80,000–160,000 h^{-1}. The HCHO concentration in inlet and outlet air was determined using phenol reagent spectrophotometry (MBTH). The HCHO degradation efficiency can be calculated as follows:

$$\text{Removal efficiency } (\%) = \frac{[\text{HCHO}]\text{in} - [\text{HCHO}]\text{out}}{[\text{HCHO}]\text{in}} \times 100\%$$

Here, $[HCHO]_{in}$ and $[HCHO]_{out}$ are the concentrations of HCHO at the inlet and outlet, respectively.

In this paper, the MBTH method was used to detect the formaldehyde content. The reagents of $C_8H_9N_3S \cdot HCl \cdot H_2O$, $NH_4Fe(SO_4)_2 \cdot 12H_2O$ and HCl were analytically pure for the MBTH method and purchased from Shanghai Macklin Biochemical Co., Ltd. (Shanghai, China). The standard working curve was made by purchasing a standard formaldehyde solution at the beginning of the test to ensure the accuracy of data.

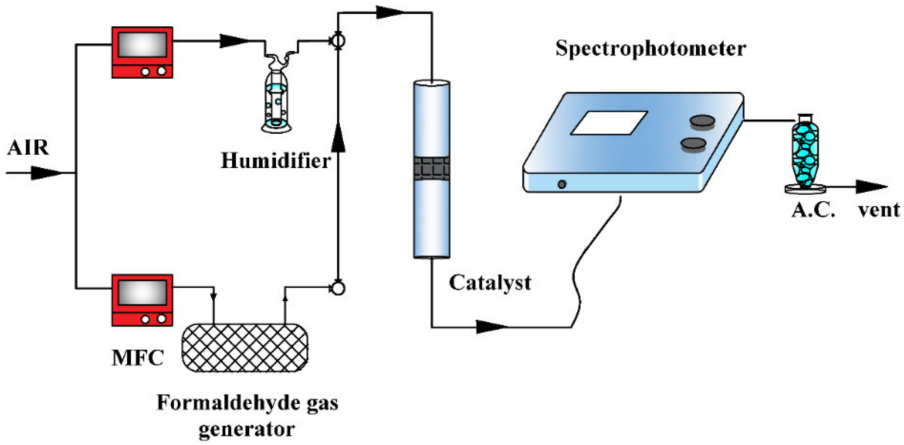

Figure 10. Schematic illustration for catalytic activity evaluation.

5. Conclusions

In this paper, the influence of pH on the δ-MnO_2 catalytic oxidation performance of formaldehyde at room temperature was investigated. The results of XRD, SEM, TEM, and BET showed the crystal plane spacing of layered δ-MnO_2 widened as the precursor solution pH rose from 7 to 13. Additionally, the crystal plane spacing was the widest, and the specific surface area and pore size were also the largest, when pH = 13. Such a structure is conducive to the formation of rich Mn vacancies and active sites, which is beneficial for the adsorption of active oxygen species and catalytic activity for formaldehyde degradation. The above conclusions were also confirmed using XPS and H_2-TPR. However, when the pH rose to 14, the lamellar structure of the catalyst disappeared, and the interlayer spacing and pore size became smaller, reducing the storage space of the active species and hindering the transport and reaction of the reactant formaldehyde. Therefore, the catalyst prepared at pH 13 had the best catalytic activity. It can be concluded that by adjusting and optimizing pH, the active site and defect structure of the catalyst can be effectively regulated, and the catalytic activity and stability of the catalyst can be improved. Considering the abundant Mn vacancies, the strong adsorption capacity for active oxygen, and the high HCHO capture capacity at low concentration and high velocity, 13-MnO_2 can be used as a very attractive option for HCHO removal at room temperature.

Author Contributions: Methodology, W.Z.; catalyst preparation, M.H.; activity evaluation, Y.W.; catalyst characterization, P.S.; activity analysis, D.Z.; writing—original draft preparation, M.H., Y.W. and X.W.; writing—review and editing, W.Z. and M.H.; funding acquisition, W.Z. and P.L. All authors have read and agreed to the published version of the manuscript.

Funding: This research was funded by the National Natural Science Foundation of China grant number 42107284 and 22078177.

Data Availability Statement: The authors confirm that the data supporting the findings of this study are available within the article.

Acknowledgments: I would like to express my gratitude to all members of our research group who helped me during the writing this study. I also would like to give my thanks to my family.

Conflicts of Interest: The authors declare no conflict of interest.

References

1. Guan, S.; Li, W.; Ma, J.; Lei, Y.; Zhu, Y.; Huang, Q.; Dou, X. A review of the preparation and applications of MnO_2 composites in formaldehyde oxidation. *J. Ind. Eng. Chem.* **2018**, *66*, 126–140. [CrossRef]
2. Yusuf, A.; Snape, C.; He, J.; Xu, H.; Liu, C.; Zhao, M.; Chen, G.Z.; Tang, B.; Wang, C.; Wang, J. Advances on transition metal oxides catalysts for formaldehyde oxidation: A review. *Catal. Rev.* **2017**, *59*, 189–233. [CrossRef]
3. Bai, B.; Qiao, Q.; Li, J.; Hao, J. Progress in research on catalysts for catalytic oxidation of formaldehyde. *Chin. J. Catal.* **2016**, *37*, 102–122. [CrossRef]

4. Zhu, S.; Wang, J.; Nie, L. Progress of catalytic oxidation of formaldehyde over manganese oxides. *ChemistrySelect* **2019**, *4*, 12085–12098. [CrossRef]
5. Ashwini, S.; Prashantha, S.C.; Naik, R.; Naik, Y.V.; Nagabhushana, H.; Narasimhamurthy, K.N. Photoluminescence and photocatalytic properties of novel Bi_2O_3:Sm^{3+} nanophosphor. *J. Sci.-Adv. Mater. Devices* **2019**, *4*, 531–537. [CrossRef]
6. Shanbhag, V.V.; Prashantha, S.; Kumar, P.; Surendra, B.; Nagabhushana, H.; Jnaneshwara, D.; Revathi, V.; Naik, R.; Shashidhara, T.; Krupanidhi, Y. Comparative analysis of electrochemical performance and photocatalysis of SiO_2 coated $CaTiO_3$: RE^{3+} (Dy, Sm), Li^+ core shell nano structures. *Inorg. Chem. Commun.* **2021**, *134*, 108960. [CrossRef]
7. Huang, Z.; Cao, S.; Yu, J.; Tang, X.; Guo, Y.; Guo, Y.; Wang, L.; Dai, S.; Zhan, W. Total oxidation of light alkane over phosphate-modified Pt/CeO_2 catalysts. *Environ. Sci. Technol.* **2022**, *56*, 9661–9671. [CrossRef]
8. Zhang, N.; Guo, Y.; Guo, Y.; Dai, Q.; Wang, L.; Dai, S.; Zhan, W. Synchronously constructing the optimal redox-acidity of sulfate and RuO_x Co-modified CeO_2 for catalytic combustion of chlorinated VOCs. *Chem. Eng. J.* **2023**, *454*, 140391. [CrossRef]
9. Feng, X.; Xia, L.; Jiang, Z.; Tian, M.; Zhang, S.; He, C. Dramatically promoted toluene destruction over Mn@ Na-Al_2O_3@ Al monolithic catalysts by Ce incorporation: Oxygen vacancy construction and reaction mechanism. *Fuel* **2022**, *326*, 125051. [CrossRef]
10. Sidheswaran, M.A.; Destaillats, H.; Sullivan, D.P.; Larsen, J.; Fisk, W.J. Quantitative room-temperature mineralization of airborne formaldehyde using manganese oxide catalysts. *Appl. Catal. B* **2011**, *107*, 34–41. [CrossRef]
11. Eckert, M.; Peters, W.; Drillet, J.-F. Fast microwave-assisted hydrothermal synthesis of pure layered δ-MnO_2 for multivalent ion intercalation. *Materials* **2018**, *11*, 2399. [CrossRef]
12. Wang, C.; Zou, X.; Liu, H.; Chen, T.; Suib, S.L.; Chen, D.; Xie, J.; Li, M.; Sun, F. A highly efficient catalyst of palygorskite-supported manganese oxide for formaldehyde oxidation at ambient and low temperature: Performance, mechanism and reaction kinetics. *Appl. Surf. Sci.* **2019**, *486*, 420–430. [CrossRef]
13. Pang, G.; Wang, D.; Zhang, Y.; Ma, C.; Hao, Z. Catalytic activities and mechanism of formaldehyde oxidation over gold supported on MnO_2 microsphere catalysts at room temperature. *Front. Environ. Sci. Eng.* **2016**, *10*, 447–457. [CrossRef]
14. Wu, Y.; Lu, Y.; Song, C.; Ma, Z.; Xing, S.; Gao, Y. A novel redox-precipitation method for the preparation of α-MnO_2 with a high surface Mn^{4+} concentration and its activity toward complete catalytic oxidation of o-xylene. *Catal. Today* **2013**, *201*, 32–39. [CrossRef]
15. Min, X.; Guo, M.; Li, K.; Gu, J.-N.; Guo, X.; Xue, Y.; Liang, J.; Hu, S.; Jia, J.; Sun, T. Enhancement of toluene removal over α@ δ-MnO_2 composites prepared via one-pot by modifying the molar ratio of $KMnO_4$ to $MnSO_4 \cdot H_2O$. *Appl. Surf. Sci.* **2021**, *568*, 150972. [CrossRef]
16. Chen, Y.; Hong, Y.; Ma, Y.; Yang, H.; Li, J. Preparation of nanostructure MnO_2 single crystal in various acid solution. *Acta Metall. Sin.* **2010**, *46*, 857–861. [CrossRef]
17. Jiang, Y.; Cheng, G.; Yang, R.; Liu, H.; Sun, M.; Yu, L.; Hao, Z. Influence of preparation temperature and acid treatment on the catalytic activity of MnO_2. *J. Solid State Chem.* **2019**, *272*, 173–181. [CrossRef]
18. Zheng, X.; Cai, J.; Cao, Y.; Shen, L.; Zheng, Y.; Liu, F.; Liang, S.; Xiao, Y.; Jiang, L. Construction of cross-linked δ-MnO_2 with ultrathin structure for the oxidation of H_2S: Structure-activity relationship and kinetics study. *Appl. Catal. B* **2021**, *297*, 120402. [CrossRef]
19. Wang, J.; Li, J.; Jiang, C.; Zhou, P.; Zhang, P.; Yu, J. The effect of manganese vacancy in birnessite-type MnO_2 on room-temperature oxidation of formaldehyde in air. *Appl. Catal. B* **2017**, *204*, 147–155. [CrossRef]
20. Miao, L.; Xie, Y.; Xia, Y.; Zou, N.; Wang, J. Facile photo-driven strategy for the regeneration of a hierarchical C@MnO_2 sponge for the removal of indoor toluene. *Appl. Surf. Sci.* **2019**, *481*, 404–413. [CrossRef]
21. Yang, W.; Su, Z.; Xu, Z.; Yang, W.; Peng, Y.; Li, J. Comparative study of α-, β-, γ-and δ-MnO_2 on toluene oxidation: Oxygen vacancies and reaction intermediates. *Appl. Catal. B* **2020**, *260*, 118150. [CrossRef]
22. Wang, J.; Zhang, G.; Zhang, P. Layered birnessite-type MnO_2 with surface pits for enhanced catalytic formaldehyde oxidation activity. *J. Mater. Chem. A* **2017**, *5*, 5719–5725. [CrossRef]
23. Zhang, H.; Zheng, X.; Xu, T.; Zhang, P. Atomically dispersed Y or La on birnessite-type MnO_2 for the catalytic decomposition of low-concentration toluene at room temperature. *ACS Appl. Mater. Interfaces* **2021**, *13*, 17532–17542. [CrossRef] [PubMed]
24. Gil, E.R.; Ruiz, B.; Lozano, M.; Martín, M.; Fuente, E. VOCs removal by adsorption onto activated carbons from biocollagenic wastes of vegetable tanning. *Chem. Eng. J.* **2014**, *245*, 80–88. [CrossRef]
25. Wang, J.; Li, D.; Li, P.; Zhang, P.; Xu, Q.; Yu, J. Layered manganese oxides for formaldehyde-oxidation at room temperature: The effect of interlayer cations. *RSC Adv.* **2015**, *5*, 100434–100442. [CrossRef]
26. Wang, Z.; Chen, B.; Crocker, M.; Yu, L.; Shi, C. New insights into alkaline metal modified CoMn-oxide catalysts for formaldehyde oxidation at low temperatures. *Appl. Catal. A* **2020**, *596*, 117512. [CrossRef]
27. Sun, D.; Wageh, S.; Al-Ghamdi, A.A.; Le, Y.; Yu, J.; Jiang, C. Pt/C@ MnO_2 composite hierarchical hollow microspheres for catalytic formaldehyde decomposition at room temperature. *Appl. Surf. Sci.* **2019**, *466*, 301–308. [CrossRef]
28. Huang, Q.; Lu, Y.; Si, H.; Yang, B.; Tao, T.; Zhao, Y.; Chen, M. Study of Complete Oxidation of Formaldehyde Over MnO x–CeO_2 Mixed Oxide Catalysts at Ambient Temperature. *Catal. Lett.* **2018**, *148*, 2880–2890. [CrossRef]
29. Chen, T.; Dou, H.; Li, X.; Tang, X.; Li, J.; Hao, J. Tunnel structure effect of manganese oxides in complete oxidation of formaldehyde. *Microporous Mesoporous Mater.* **2009**, *122*, 270–274. [CrossRef]

30. Tian, Y.; Li, D.; Liu, J.; Wang, H.; Zhang, J.; Zheng, Y.; Liu, T.; Hou, S. Facile synthesis of Mn_3O_4 nanoplates-anchored graphene microspheres and their applications for supercapacitors. *Electrochim. Acta* **2017**, *257*, 155–164. [CrossRef]
31. Zhao, W.; Cui, H.; Liu, F.; Tan, W.; Feng, X. Relationship between Pb^{2+} adsorption and average Mn oxidation state in synthetic birnessites. *Clays Clay Miner.* **2009**, *57*, 513–520. [CrossRef]
32. Yusuf, A.; Sun, Y.; Ren, Y.; Snape, C.; Wang, C.; Jia, H.; He, J. Opposite effects of Co and Cu dopants on the catalytic activities of birnessite MnO_2 catalyst for low-temperature formaldehyde oxidation. *J. Phys. Chem. C* **2020**, *124*, 26320–26331. [CrossRef]
33. Fang, R.; Huang, H.; Ji, J.; He, M.; Feng, Q.; Zhan, Y.; Leung, D.Y. Efficient MnO_x supported on coconut shell activated carbon for catalytic oxidation of indoor formaldehyde at room temperature. *Chem. Eng. J.* **2018**, *334*, 2050–2057. [CrossRef]
34. Zheng, J.Y.; Zhao, W.K.; Wang, X.; Zheng, Z.; Zhang, Y.; Wang, H.; Yan, H.; Song, X.; Han, C.B. Electric-enhanced hydrothermal synthesis of manganese dioxide for the synergistic catalytic of indoor low-concentration formaldehyde at room temperature. *Chem. Eng. J.* **2020**, *401*, 125790. [CrossRef]
35. Chen, J.; Tang, H.; Huang, M.; Yan, Y.; Zhang, J.; Liu, H.; Zhang, J.; Wang, G.; Wang, R. Surface lattice oxygen activation by nitrogen-doped manganese dioxide as an effective and longevous catalyst for indoor HCHO decomposition. *ACS Appl. Mater. Interfaces* **2021**, *13*, 26960–26970. [CrossRef]
36. Rong, S.; Li, K.; Zhang, P.; Liu, F.; Zhang, J. Potassium associated manganese vacancy in birnessite-type manganese dioxide for airborne formaldehyde oxidation. *Catal. Sci. Technol.* **2018**, *8*, 1799–1812. [CrossRef]
37. Kim, S.C.; Shim, W.G. Catalytic combustion of VOCs over a series of manganese oxide catalysts. *Appl. Catal. B* **2010**, *98*, 180–185. [CrossRef]
38. Ma, C.; Sun, S.; Lu, H.; Hao, Z.; Yang, C.; Wang, B.; Chen, C.; Song, M. Remarkable MnO_2 structure-dependent H_2O promoting effect in HCHO oxidation at room temperature. *J. Hazard. Mater.* **2021**, *414*, 125542. [CrossRef]
39. Zhou, L.; Zhang, J.; He, J.; Hu, Y.; Tian, H. Control over the morphology and structure of manganese oxide by tuning reaction conditions and catalytic performance for formaldehyde oxidation. *Mater. Res. Bull.* **2011**, *46*, 1714–1722. [CrossRef]
40. Qi, Q.; Zhang, W.; Zhang, Y.; Bai, G.; Liang, P. Formaldehyde oxidation at room temperature over layered MnO_2. *Catal. Commun.* **2021**, *153*, 106293. [CrossRef]